Nano-Structures & Nano-Objects 4 (2015) 9–14

Contents lists available at ScienceDirect

Nano-Structures & Nano-Objects

journal homepage: www.elsevier.com/locate/nanoso

Preparation and microscopic characterization of magnetite–gold mesoparticles with tunable morphology

Paulina Lloret [a], Gabriel Ybarra [a], Pablo Granell [b], Leandro Socolovsky [c], Carlos Moina [a,*]

[a] Unidad Técnica Nanomateriales, INTI-Procesos Superficiales, Instituto Nacional de Tecnología Industrial, San Martín, Argentina
[b] Centro de Micro y Nanoelectrónica del Bicentenario, Instituto Nacional de Tecnología Industrial, San Martín, Argentina
[c] Laboratorio de Sólidos Amorfos, Facultad de Ingeniería, Universidad de Buenos Aires, Argentina

HIGHLIGHTS

- Magnetite-gold mesoparticles were prepared with controlled morphology by adjusting the concentration of reactants and surfactants used in the synthesis.
- A structural study was carried out by using FIB/SEM technology which revealed that the inner structured of the particles is composed by iron oxide nanoparticles and gold crystals.
- A tridimensional reconstruction was created from SEM images of sliced mesoparticles by focused ion beam.

GRAPHICAL ABSTRACT

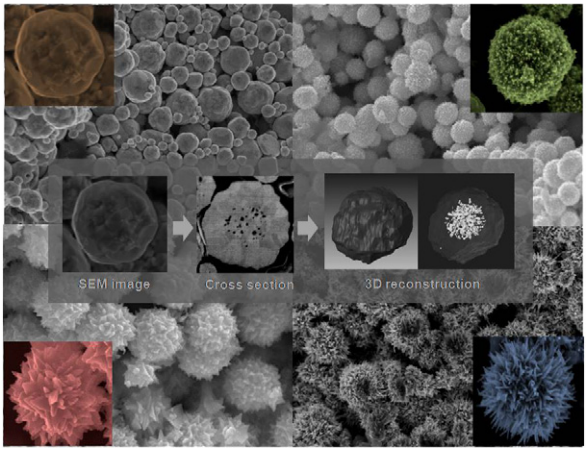

ARTICLE INFO

Article history:
Received 13 July 2015
Accepted 25 October 2015

Keywords:
Magnetite
Gold
Mesoparticles

ABSTRACT

Composite magnetite–gold mesoscopic particles were prepared by deposition of Au onto magnetite nanoparticles. The surface morphology of the mesoparticles could be tuned by controlling the factors that affect the kinetics of the reactions and by adding surfactants that direct the growth of gold crystals. The internal structure of composite mesoparticles was analyzed by focused ion beam and scanning electron microscopy. A particle-mediated growth mechanism of formation was proposed.

© 2015 Elsevier B.V.
This is an open access article under the CC BY-NC-ND license (http://creativecommons.org/licenses/by-nc-nd/4.0/).

1. Introduction

Despite their impressive wealth of applications [1–4], nanoparticles present drawbacks inherent to their nanoscale condition [5]. Their high area to volume ratio and extremely small size make them prone to suffer from problems in terms of thermal stability, shape preservation, and manipulation. One of the strategies currently being developed to mitigate these problems consists in the preparation of larger particles that only some of the properties characteristic of nanoscale materials are preserved. Therefore in recent years, there has been an increasing interest in the synthesis, characterization and applications of particles with a size in the mesoscale (roughly between 100 nm and 1 μm). Considerable effort has been made in order to obtain mesoscopic particles (mesoparticles) of controlled size and morphology formed by the

* Corresponding author.
E-mail address: moina@inti.gov.ar (C. Moina).

http://dx.doi.org/10.1016/j.nanoso.2015.10.002
2352-507X/© 2015 Elsevier B.V. This is an open access article under the CC BY-NC-ND license (http://creativecommons.org/licenses/by-nc-nd/4.0/).

controlled aggregation of nanoparticles [6]. Mesoparticles prepared in such a way are expected to show a higher stability and to be easier to handle, while other nanoscale properties are expected to be retained.

Important progress has been recently made in the preparation and the understanding of the mechanism of growth of mesoscopic particles formed by the aggregation of nanoparticles, especially regarding the formation of metallic mesocrystals [7]. A mesocrystal is a mesoscopic particle composed by a number of individual nanocrystals aligned along a common crystallographic direction, forming an ordered mesoscale superstructure [8]. A mechanism of formation has been proposed for gold [9] as well as for silver metallic mesocristals [10]. The proposed mechanism involves four stages: initially, Au atoms are formed by chemical reduction; subsequently, Au atoms aggregate and form nuclei; then metallic nuclei aggregate to form mesoparticles in a process called particle-mediated growth; finally, Au atoms deposit onto the mesoparticle defining the final morphology of the mesoparticle. The final phase is called overgrowth and can be chemically controlled so that the resulting morphology can be tuned.

The preparation of magnetite microparticles of controlled surface morphology and internal structure has also been recently reported [11]. The authors proposed a particle-mediated growth mechanism which shares similarities with the one proposed for metallic mesoparticles: under appropriate conditions, nuclei are formed and then aggregate, while the morphology and size of the particles is defined during the overgrowth (in this phase, Ostwald ripening can also take place and modify the internal structure of the particle; this process is not possible for metallic mesocrystals).

Few studies have focused on the formation of mesoparticles composed by two dissimilar materials, such as magnetite and gold [12–15]. Moreover, a microscopic characterization of their internal structure has never been carried out and the mechanism of formation has not been properly discussed. In this paper, we present the preparation of magnetite and gold mesoparticles with tunable morphology, characterize their surface morphology and internal structure by scanning electron microscopy (SEM) and focused ion beam (FIB), and propose a particle-mediated growth mechanism of formation of mesoparticles.

2. Experimental

2.1. Synthesis of the mesoparticles

A co-precipitation method was used to obtain Fe_3O_4. 12 g of $FeCl_3.6H_2O$ were dissolved in 75 ml of deionized water and 6 g of $FeCl_2.4H_2O$ dissolved in 25 ml of deionized water was added. 25 ml of concentrated ammonium hydroxide was dropped into the iron solution with stirring. A black precipitate was obtained and washed four times with the aid of a permanent magnet. Then, 30 mg of Fe_3O_4 were added to 80 ml of a solution of toluene containing 3.5 mM of oleic acid and c mM of oleylamine, with $c = 1.2$, 2.4 and 24 mM and redispersed with ultrasonic agitation.

Four different types of mesoparticles were prepared. For the synthesis of the Type I and II particles, a solution of gold in toluene was obtained by dissolving 0.13 mmol of Au from $KAuCl_4.xH_2O$ (49% Au, Aldrich) in 20 ml of 2-propanol and then added to 100 ml of toluene.

For synthesis of Type III and Type IV particles, a solution of 0.13 mmol of $KAuCl_4.xH_2O$ (49% Au, Aldrich) in 40 ml of water was extracted with 100 ml of 1.5 mM solution of tetraoctylammonium bromide.

In all cases, the magnetic dispersion was added to the organic gold solution and 5.9 mM of hydroquinone dissolved in 20 ml of 2-propanol were added.

Mesoparticles were obtained after 12 h of reaction. Particles were collected with a permanent magnet and washed with toluene and 2-propanol and dried under vacuum.

2.2. Microscopic characterization

The structure of the Type I and Type III particles was characterized with a FEI Helios Nanolab 650 Scanning Electron Microscope/Focused Ion Beam (FIB/SEM) dual system. For 3D reconstruction of Type I mesoparticles, a set of high resolution SEM images was obtained from equally spaced FIB cross sections in an automated process. The images were then aligned and color segmented with an image processing software, and the volumes were rendered. In the sample preparations, a protective Pt layer of about 1–2 μm was deposited before ion beam milling. To study the particle structure by scanning transmission electron microscopy (STEM), thin lamellae of the sample were extracted and attached in-situ to a TEM half-grid by FIB milling and Pt deposition. The lamella was then thinned and polished to a final thickness of about 50 nm, suitable for STEM imaging. Electron diffraction images were taken with a Philips CM200 TEM microscope.

3. Results

Magnetite–gold mesoparticles have been prepared by the reduction of $AuCl_4^-$ in a dispersion of magnetite nanoparticles stabilized by oleylamine and oleic acid. Hydroquinone has been used as a reducing agent. Fig. 1 shows SEM images of mesoparticles prepared under different conditions. The morphology of the synthesized magnetite–gold mesoparticles could be controlled by the concentration of oleylamine and TOAB. Roughly spherical mesoparticles were obtained when an oleylamine concentration of 1.2 mM was used in the absence of TOAB (Type I particles). When the concentration of oleylamine was increased up to 2.4 mM in the absence of TOAB, mesoparticles with small gold protuberances of about 30 nm in the surface (Type II particles) were obtained. The presence of TOAB has a strong effect in the morphology of the mesoparticles. When an oleylamine concentration of 2.4 mM and a TOAB concentration of 1.5 mM were used, mesoparticles with a flower-like morphology were obtained (Type III particles), showing large pyramidal protuberances of gold. When the concentration of oleylamine was increased to 24 mM, keeping the TOAB concentration at 1.5 mM, nearly spherical mesoparticles with thin gold thorns were obtained (Type IV particles).

From these results, it is clear that oleylamine and TOAB play a key role in the fine tuning of the morphology of the mesoparticles. Oleylamine, in the absence of TOAB, promotes the formation of protuberances, as can be seen comparing Type I and Type II particles, where the oleylamine concentration was increased approximately four times. When TOAB is present in the synthesis media, the mesoparticles develop large protuberances, pyramidal at low TOAB concentrations corresponding to Type III particles and thorn-like at high TOAB concentrations corresponding to Type IV particles. In fact, the morphology of the prepared mesoparticles can be continuously varied among the structures shown in Fig. 1 by controlling the concentration of oleylamine and TOAB in the reaction media. (See supplementary information.)

It is worth noting that no free magnetite nanoparticles could be seen in these images. Since these mesoparticles presented a superparamagnetic behavior similar to that found for magnetite nanoparticles, it can be concluded that magnetite nanoparticles were present in the interior of the mesoparticles. In order to elucidate the question of the presence of the magnetite nanoparticles, as well as the internal structure of the mesoparticles, focused ion beam was used to progressively remove slices of a single mesoparticle, while the resulting sliced mesoparticle was observed by scanning electron microscopy (see Fig. 2).

It must be noted that internal structure of whole gold–magnetite mesoparticles could not be studied by TEM, because the presence

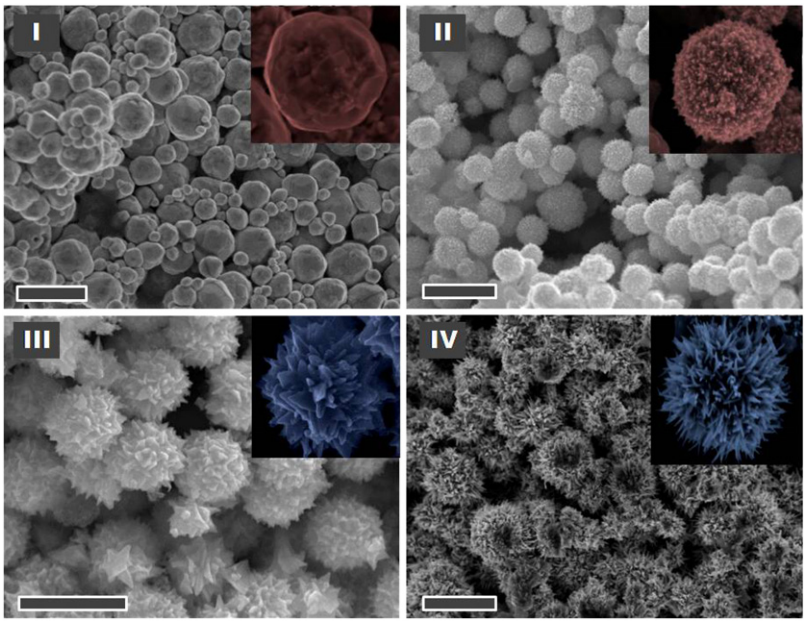

Fig. 1. SEM images of different obtained mesoparticles. The morphology was determined by the concentration of oleylamine and TOAB used in the synthesis. Particles Type I and II were obtained with a concentration of oleylamine of 1.2 mM and 2.4 mM, respectively, in the absence of TOAB. A concentration of oleylamine of 2.4 and 24 mM was used during the synthesis of particles Type III and IV respectively, while the concentration of TOAB was 1.5 mM. The scale bars represent 1 μm.

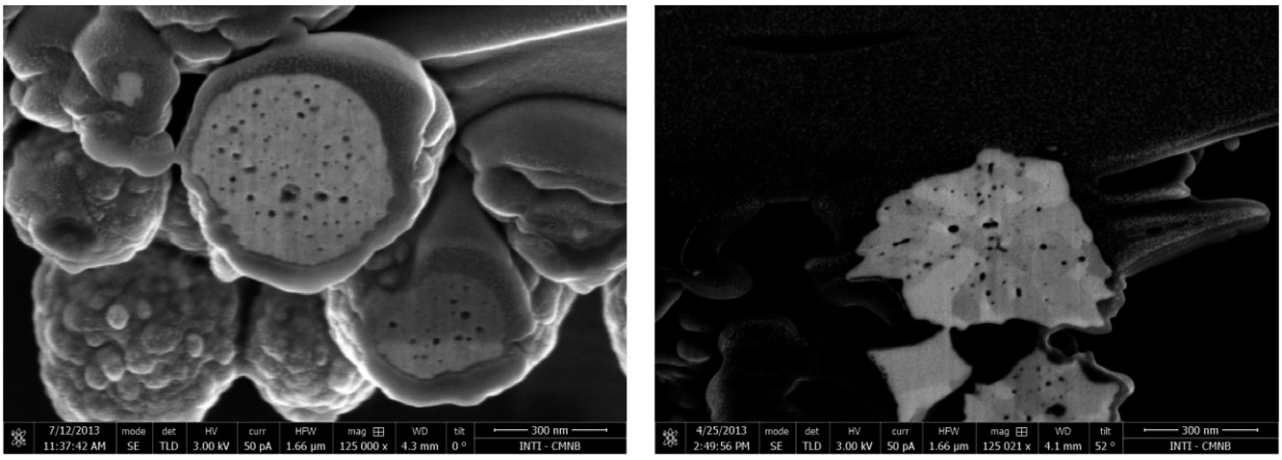

Fig. 2. SEM images of FIB cross section for a Type I (a) and Type III (b) mesoparticles.

of a thick shell of gold completely blocks the magnetite nanoparticles. Therefore, only the dark silhouette of these mesoparticles can be seen in TEM images. The thickness of the sample must be transparent enough for the incoming electron beam to be observed. Suitable thickness depends on the material and beam energy to be analyzed. In the case of materials containing gold crystals, sample should have thickness lower than 100 nm, otherwise electrons are completely scattered by the sample.

STEM images (Fig. 3) have been acquired of two slices of Type I and III mesoparticles, whose synthesis differs basically in the TOAB content. Gold crystalline domains can be seen in both types of particles, indicating that each mesoparticle was formed by multiple gold crystals. The size and shape of the crystalline domains can be clearly seen. Type III particles, whose synthesis media contains TOAB, exhibit relatively large crystal domains and straight grain boundaries, while the inner structure of Type I particles (prepared in the absence of TOAB) seem to be more irregular.

In Fig. 4, the progression of successive images obtained of a single mesoparticles (corresponding to a particle extracted from the same group as those shown in Fig. 1(a)) is shown. It can be seen that, in the first images corresponding to the outer shell of the mesoparticle, only a compact shell can be observed. Grain boundaries can be seen, indicating that this shell is composed by several gold crystals. As the slicing progresses and the core of the particle becomes apparent, a more chaotic structure is revealed, presenting voids of about 10–20 nm, a size compatible with that of magnetite nanoparticles. Thus, FIB-SEM images suggest a core formed by gold and magnetite nanoparticles surrounded by a shell of compact gold, as can be seen in a 3D reconstruction carried out from FIB-SEM images (Fig. 5).

Electron diffraction images of samples Type I and Type III taken on each respective lamellae shows spots and faint halos coming from gold and iron oxide crystals (Fig. 6). Those spots also show that in each lamella crystals of different orientations coexist, as is observed in STEM images. These results confirm the presence of magnetite nanoparticles embedded into gold crystals.

In the following section, we propose a mechanism of formation of the mesoparticles based on the FIB-SEM images, as well on the existing literature on the formation of metallic mesoparticles. The fine tuning of the morphology of the mesoparticles can also be understood in the frame of the proposed mechanism.

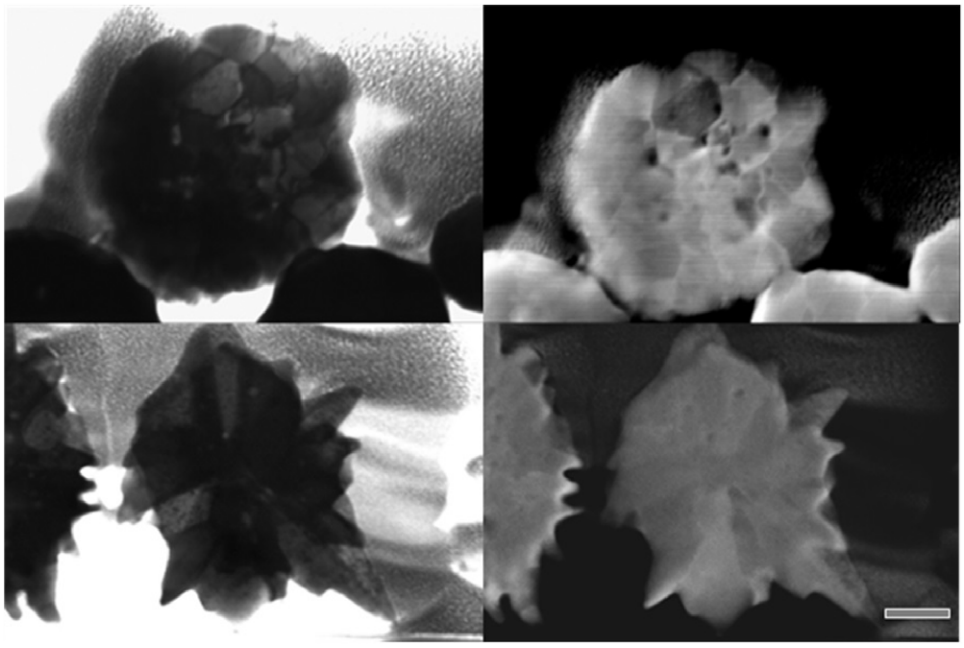

Fig. 3. STEM images of 100 nm thick lamellae of Type I and Type III particles, where the contrast between different crystalline domains can be seen in HAADF mode. The scale bars represent 100 nm.

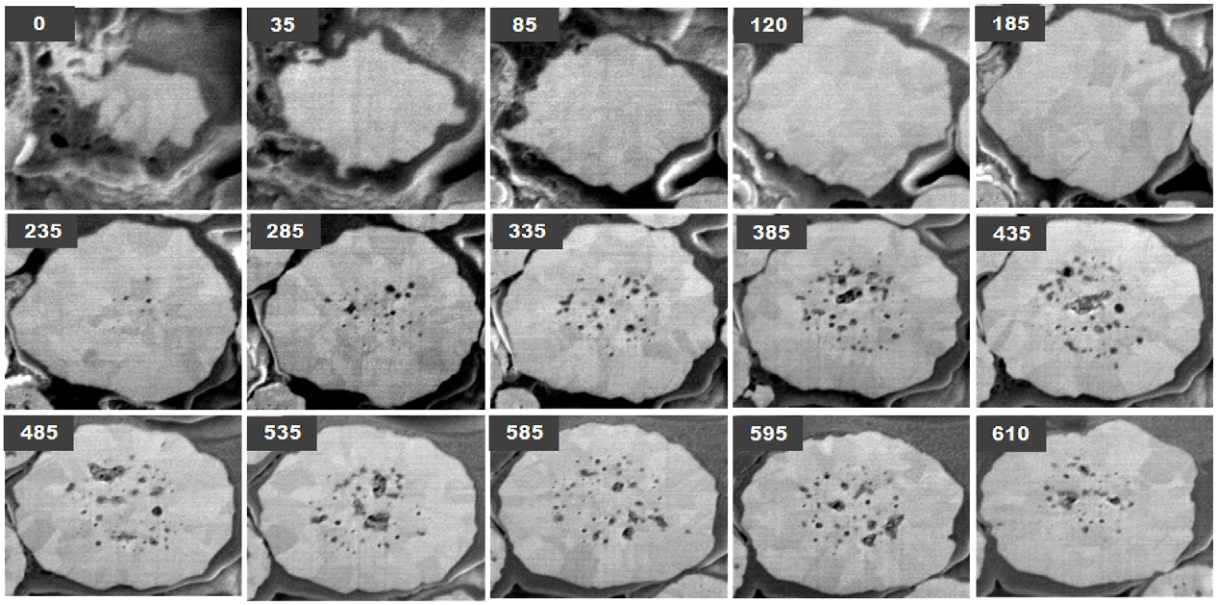

Fig. 4. SEM images of progressive cross sections obtained by FIB for a Type I mesoparticle. Images for 120 cross sections were obtained, with a difference of 5 nm between two successive images. The accumulated distance of removal is shown in nanometers at the top left corner.

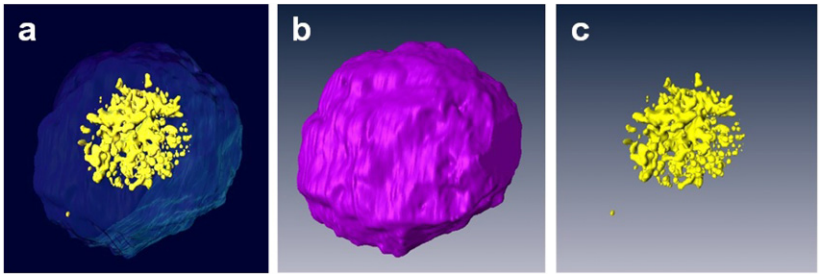

Fig. 5. (a) 3D reconstruction of mesoparticle Type I obtained from 120 images of cross sections. The image analysis software allows to distinguish two different regions, corresponding to a porous core (c) surrounded by a compact gold shell (b).

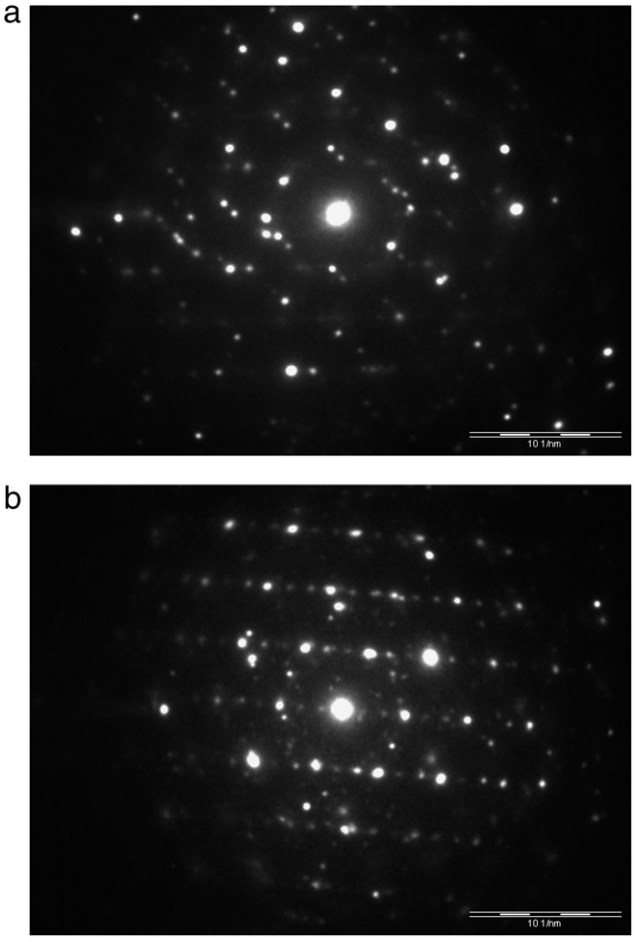

Fig. 6. Bright spots can be seen in electron diffraction images corresponding to Type I (a) and Type III (b). In both images crystalline planes {111} and {222} coming from gold crystals; and {220}, {440} and {311} family planes coming from magnetite crystals can be identified.

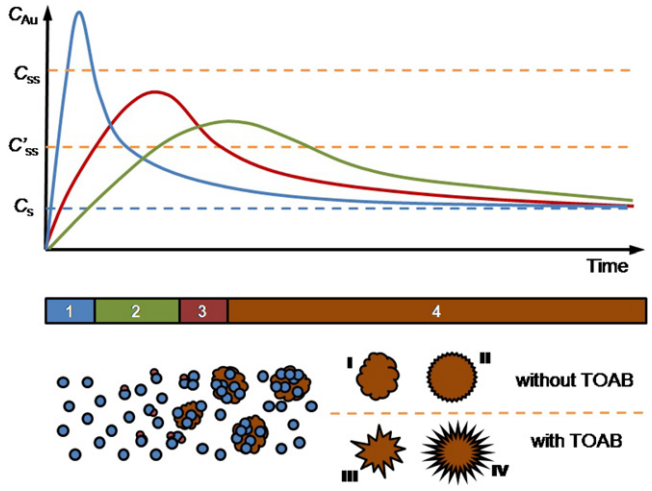

Fig. 7. Time evolution of the concentration of Au atoms in the reaction medium (above) and schematic representation of the formed particles (below) at the different stages of the reaction: (1) formation of Au atoms; (2) deposition of Au atoms onto magnetite nanoparticles; (3) aggregation of nanoparticles (particle-mediated growth); (4) overgrowth (deposition of Au atoms onto mesoparticles). The fine tuning of the topography is defined during the overgrowth by the concentration of oleylamine and TOAB. The different curves correspond to the time evolution of Au atoms under the different conditions which lead to the formation of gold mesocrystals (in blue) and gold–magnetite mesoparticles (Type I and II are shown in red, Type III and IV in green). (For interpretation of the references to colour in this figure legend, the reader is referred to the web version of this article.)

4. Discussion

We propose a mechanism based on the non-classical particle-mediated growth mechanism previously reported for the formation of silver and gold mesocrystals [9,16]. Unlike the reported cases in which only a kind of material is considered (e.g. either Au or Ag), the gold–magnetite mesoparticles are composed by two different materials. Consequently, additional processes should be taken into account, such as the heterogeneous deposition of Au atoms onto magnetite nanoparticles.

The proposed mechanism of formation of mesoparticles is illustrated in Fig. 7. Initially, a dispersion of magnetite nanoparticles stabilized with oleic acid and oleylamine is placed in contact with $AuCl_4^-$ and a reducing agent. Other components, such as TOAB, may or may not be present to the reaction medium. The proposed mechanism of particle-mediated growth can be divided in four stages. In the first stage, Au atoms are formed by the reduction of Au(III) with a reducing agent. As this reaction proceeds, the concentration of Au atoms in the solution increases, as is shown in the schematic LaMer diagram. When it exceeds the supersaturation point (C'_{ss} in Fig. 7), the second stage begins in which Au atoms deposit onto magnetite nanoparticles. This is an important difference with respect to the formation of metallic mesocrystals composed by a single metal, where metallic atoms must aggregate to form nuclei. The deposition of Au atoms onto magnetite nanoparticles is a heterogeneous phase deposition, while the formation of metallic nuclei follows the classical homogeneous precipitation process. As a consequence of the heterogeneous phase deposition of Au atoms onto magnetite nanoparticles, the concentration of Au atoms in the solution decreases. It becomes apparent that the deposition of gold onto magnetite nanoparticles disrupts the oleic acid and oleylamine cap which stabilizes the dispersion of nanoparticles, thus promoting the formation of gold–magnetite aggregates. Then, the third stage, called particle-mediated growth, begins, in which gold–magnetite nanoparticles aggregate to form roughly spherical mesoparticles. As shown in Figs. 4 and 5, this aggregation results in a rather disordered structure, well reflected in the reconstruction shown in Fig. 5. Below the supersaturation point for the heterogeneous deposition, Au atoms cease to deposit onto magnetite nanoparticles. At this point, the fourth stage, called overgrowth, begins, in which the remaining Au atoms are deposited onto the mesoparticles formed during the previous stage, inducing the overgrowth. The final morphology of the mesoparticles is defined during the overgrowth, in which gold is deposited onto magnetite–gold mesoparticles. In this stage, well-defined gold crystal developed, surrounding the less structured gold–magnetite nucleus (Fig. 4). In this stage, the presence of different compounds, which can affect the rate of deposition of gold (e.g. oleylamine and TOAB), is relevant.

It has been shown that the strength of reducing agent affects the kinetics of formation of particles, and therefore the resulting morphology [17]. As a part of this work, a synthesis using a strong reducing agent such as sodium borohydride has been carried out and it led to the formation of bluish non-magnetic particles, which can be attributed to the formation of pure gold particles. This process is also included in Fig. 7. When a strong reducing agent such as sodium borohydride is used, gold atoms are rapidly produced. Consequently, the supersaturation concentration (C_{ss} in Fig. 7) is exceeded and pure gold nuclei are formed. In order to promote the deposition of gold onto magnetite, milder reducing agents must be used so that the more sluggish kinetics which lead to the formation of composite mesoparticles can be followed. Hydroquinone was chosen because it is a mild reducing agent soluble in the toluene and 2-propanol media of reaction. In the

absence of TOAB, gold atoms are formed according to the following reaction:

$$2AuCl_4^- + 3C_6H_6O_2 \rightarrow 2Au + 3C_6H_4O_2 + 6H^+ + 8Cl^-. \quad (1)$$

This is the first stage in the path to the formation of Type I and II mesoparticles. Even though the reduction with hydroquinone is slow compared to borohydride, the reaction still proceeds at a fast rate and magnetite–gold particles have been observed after only a few minutes of reaction.

The addition of TOAB affects the process of formation of mesoparticles in two ways: firstly, by lowering the rate of formation of Au atoms and, secondly, by adsorbing onto Au facets and promoting preferential crystalline growth. In the case of Type III and IV particles, in the first step of reduction of Au (III) an exchange of ligands takes place in the $AuCl_4^-$, bromide ions replace chloride ions, and $AuBr_4^-$ is formed [18,19]. $AuBr_4^-$ is a rather stable complex and consequently the reduction of Au(III) and the formation of gold atoms is slower in the presence of TOAB since the following reaction is more sluggish:

$$2AuBr_4^- + 3C_6H_6O_2 \rightarrow 2Au + 3C_6H_4O_2 + 6H^+ + 8Br^-. \quad (2)$$

As a consequence, the formation of mesoparticles proceeds at a slower rate and only after two hours the first particles could be observed. On the other hand, bromide has a tendency to adsorb to gold crystalline planes, promoting anisotropic growth [20,21]. It is well known that bromide ions adsorb preferentially onto (111) planes, which leads to the formation of pyramidal crystalline tips [22]. To test the influence of the amine groups on the formation of pyramidal tips, a preparation of particles was carried out in which CTAB (cetrimonium bromide) was used in place of TOAB. Particles with pyramidal tips were also obtained, suggesting that this morphological feature is determined by the presence of bromide anions and the corresponding organic cation plays a secondary role.

The content of oleylamine also affects the overgrowth of mesoparticles. Oleylamine is known to promote the formation of nanowires. Similarly, increasing amounts of oleylamine promote the formation of protuberances (Type II particles) and thorns (Type IV particles) in magnetite–gold mesoparticles. Thus, in the absence of bromide, it is possible to gradually modify the surface topography of the smooth surface of Type I particles to the rough one of Type II particles by increasing the oleylamine concentration. In the presence of bromide, the surface topography can be tuned from the pyramids that cover Type III particles to the thorns of Type IV particles.

5. Conclusions

Composite magnetite–gold mesoparticles were prepared in a one-pot method. The surface morphology of the mesoparticles could be tuned by controlling the factors that affect the kinetics of the reactions (i.e. the rate of gold atoms formation) and by adding surfactants that direct the anisotropic growth of gold crystals. The internal structure of composite mesoparticles was analyzed for the first time by FIB-SEM and a mechanism of formation was proposed in accordance with the observed characteristics of the particles and the existing literature.

Acknowledgments

The authors thank Gonzalo Zbihlei from CNEA for TEM images. LMS thanks CONICET.

References

[1] S.Y. Shim, D.K. Lim, J.M. Nam, Nanomedicine 3 (2008) 215.
[2] X. Liu, Q. Dai, L. Austin, J. Coutts, G. Knowles, J. Zou, J. Am. Chem. Soc. 130 (2008) 2780.
[3] G. Han, P. Ghosh, V.M. Rotello, Nanomedicine 2 (2007) 113.
[4] A.K. Salem, P.C. Searson, K.W. Leong, Nature Mater. 2 (2003) 668.
[5] K. Okuyama, M. Abdullah, I.W. Lenggoro, F. Iskandar, Adv. Powder Technol. 17, 6 (2006) 587.
[6] M. Niederberger, H. Colfen, Phys. Chem. Chem. Phys. 8 (2006) 3271.
[7] J. Fang, S. Du, S. Lebedkin, Z. Li, R. Kruk, M. Kappes, H. Hahn, Nano Lett. 10 (2010) 5006.
[8] J. Fang, B. Ding, H. Gleiter, Chem. Soc. Rev. 40 (2011) 5347.
[9] referencia oro J. Xie, Q. Zhang, J. Yang Lee, D. Wang, ACS NANO 2 (12) (2008) 2473.
[10] L. Cheng, C. Ma, G. Yang, H. You, J. Fang, J. Mater. Chem. A 2 (2014) 4534.
[11] B. Rodríguez-González, F. Vereda, J. de Vicente, R. Hidalgo-Álvarez, J. Phys. Chem. C 117 (2013) 5397.
[12] P. Lloret, G. Longinotti, G. Ybarra, L. Socolovsky, C. Moina, Mater. Res. Bull. 48 (10) (2013) 3671.
[13] Z. Yang, Z. Hong Lin, C. Tang, H. Chang, Nanotechnology 18 (2007) 255606.
[14] Y. Wei, R. Klajn, A.O. Pinchuk, B.A. Grzybowski, Small 4 (2008) 1635.
[15] Q. Wei, H. Song, A.P. Leonov, J.A. Hale, D. Oh, Q.K. Ong, K. Ritchie, A. Wei, J. Am. Chem. Soc. 131 (28) (2009) 9728.
[16] H. You, Y. Ji, L. Wang, S. Yang, Z. Yang, J. Fang, X. Song, B. Ding, J. Mater. Chem. 22 (2012) 1998.
[17] M.R. Langille, M.L. Personick, J. Zhang, C.A. Mirkin, J. Am. Chem. Soc. 134 (2012) 14542.
[18] G.H. Woehrie, L.E. Brown, J.E. Hutchinson, J. Am. Chem. Soc. 127 (2005) 2172.
[19] L. Wang, J. Luo, M.M. Maye, Q. Fan, Q. Redeng, M.H. Engelhard, C. Wang, Y. Lin, C.J. Zhong, J. Mater. Chem. 15 (2005) 1821.
[20] H. Senapati, A.K. Singh, S.A. Khan, T. Senapati, P.C. Ray, Chem. Phys. Lett. 504 (2011) 46.
[21] T.K. Sau, C.J. Murphy, J. Am. Chem. Soc. 126 (2004) 8648.
[22] H.L. Wu, C.H. Chen, M. Huang, Chem. Mater. 21 (2009) 110.